International Journal of Multiphase Flow 35 (2009) 840–853

Contents lists available at ScienceDirect

International Journal of Multiphase Flow

journal homepage: www.elsevier.com/locate/ijmulflow

Review

Agglomeration of inertial particles in a random rotating symmetric straining flow

Yasmine Ammar [a,b], Michael Reeks [a,*]

[a] School of Mechanical and Systems Engineering, Stephenson Building, Claremont Rd, Newcastle University, Newcastle upon Tyne NE1 7RU, UK
[b] Thermal-Hydraulics Laboratory, Nuclear Energy and Safety Department, Paul Scherrer Institute, CH-5232, Villigen PSI, Switzerland

ARTICLE INFO

Article history:
Received 6 June 2008
Received in revised form 30 April 2009
Accepted 1 May 2009
Available online 23 May 2009

Keywords:
Agglomeration
Segregation
Turbulence

ABSTRACT

This paper is concerned with the development and validation of a simple Lagrangian model for particle agglomeration in a turbulent flow involving the collision of particles in a sequence of correlated straining and vortical structures which simulate the Kolmogorov small scales of motion of the turbulence responsible for particle pair dispersion and collision. In this particular study we consider the collision rate of monodisperse spherical particles in a symmetric (pure) straining flow which is randomly rotated to create an isotropic flow. The model is similar to the classical model of Saffman and Turner (S&T) (1956) for the collision (agglomeration) of tracer particles suspended in a turbulent flow. However unlike S&T, the straining flow is not frozen in time persisting only for timescales ~Kolmogorov timescale. Furthermore, we consider the collision of inertial particles as well as tracer particles, and study their behavior not only at the collision boundary but also in its vicinity. In the simulation, particles are injected continuously at the boundaries of the straining flow, the size of the straining region being typical of the Kolmogorov length scale η_K of the turbulence. For steady state conditions, we calculate the flux of particles colliding with a test particle at the centre of the straining flow and consider its dependence on the inertia of the colliding particles (characterized by the particle Stokes number, St). The model replicates the segregation and accumulation observed in DNS and in particular the maximum segregation for $St \sim 1$ (where St is the ratio of the particle response time to the Kolmogorov timescale). We also calculate the contributions of the various turbulent forces in the momentum balance equation for satellite particles and show for instance that for small Stokes number, there is a balance between turbulent diffusion and turbophoresis (gradient of kinetic stresses) which in turn is responsible for the build-up of concentration at the collision boundary. As found in previous studies, for the case of inertialess tracer particles, the collision rate turns out to be significantly smaller than the S&T prediction due to a lowering of the concentration at the collision boundary compared to the fully mixed value. The increase in collision rate for $St \sim 0.5$ is shown to be a combination of particle segregation (build-up of concentration near the collision boundary) and the decorrelation of the relative velocity between the local fluid and a colliding particle. The difference from the S&T value for the agglomeration kernel is shown to be a consequence of the choice of perfectly absorbing boundary conditions at collision and the influence of the time scale of the turbulence (eddy lifetime). We draw the analogy between turbulent agglomeration and particle deposition in a fully developed turbulent boundary layer.

© 2009 Elsevier Ltd. All rights reserved.

1. Introduction

The agglomeration of small particles suspended in a turbulent flow plays an important role in many environmental and industrial processes from mixing and combustion to droplet coalescence and precipitation in clouds (Shaw et al., 1998; Pinsky and Khain, 2000; Vaillancourt and Yau, 2000; Falkovich et al., 2002; Wang and Ayala, 2005). Our particular interest is motivated by the important role agglomeration can play in reducing the emission of radioactive aerosol in a severe nuclear accident since agglomeration reduces the timescale for aerosol deposition due to gravitational settling within the reactor containment with a consequent reduction in the release to the environment.

The particular study we present here is in fact part of a long term program of research concerned with both agglomeration and de-agglomeration (breakup), since turbulent structures in the flow have the potential to breakup agglomerates as well as increase the agglomerate collision rate. Both these features have been measured in the ARTIST experiment which simulates the initial phase of release of nuclear aerosols from a Steam Generator Tube Rupture in the secondary circuit of a PWR (Güntay and Suckow, 2004). Current models in severe accident codes only account for aerosol agglomeration (not breakup) and are based on the classical Saffman and Turner (1956) (S&T) model which among other things assumes that particles are inertialess (i.e. follow the small scale structures of the flow that are responsible for agglomeration)

* Corresponding author. Tel.: +44 191 222 3570; fax: +44 191 222 8600.
E-mail address: Mike.Reeks@ncl.ac.uk (M. Reeks).

0301-9322/$ - see front matter © 2009 Elsevier Ltd. All rights reserved.
doi:10.1016/j.ijmultiphaseflow.2009.05.005

and that no breakup occurs once an agglomerate is formed. In most cases, neither is the case, so there is a need to develop a simple model that is appropriate for both agglomeration and breakup which accounts for the influence of particle inertia. From a practical point of view such a model should also be readily incorporated into a nuclear safety code, be computationally fast and efficient and therefore not rely on the DNS of turbulence for its implementation but replicate in a mechanistic way the underlying features of agglomeration and mixing for inertial particles as revealed in many DNS studies.

Contrary to expectation, inertial particles released into a turbulent flow do not mix but segregate into the straining regions in the flow between the regions of vorticity (Crowe et al., 1993). The scale of the segregation is typically associated with the small scales of the turbulence which contain the highest straining rates in the flow, i.e. the Kolmogorov scales. The rate of segregation depends upon the particle Stokes number defined as the particle response time (Stokes relaxation time) compared to the typical timescale of the flow (in this case the Kolmogorov timescale) and reaches a maximum rate when the particle Stokes number $(St) \sim 1$. The Stokes number here is thus a measure of particle inertia.

Particle segregation (preferential concentration) by turbulent structures has been the subject of considerable research in the last 20 years, beginning with the work of Maxey (1987), Squires and Eaton (1991), Fung (1993) and Wang and Maxey (1993) who identified and quantified the process and more recently with the work of Falkovich et al. (2002), Bec (2005), Wilkinson et al. (2006) and Ijzermans et al. (submitted for publication) who revealed and quantified its multi fractal and intermittent nature (associated with the compressibility of the underlying particle velocity field and the existence of singularities (caustics) in the particle concentration field). In parallel with these investigations, there have been a number of seminal studies (Sundaram and Collins, 1997; Reade and Collins, 2000; Brunk et al., 1998; Chun et al., 2005; Wang et al., 1998a,b, 2005). Zaichik and Alipchenkov (2003), Zaichik and Simonin (2006) who through a combination of DNS, kinematic simulation and modeling have investigated in detail how the segregation process enhances particle collision rates. The focus has been on two particle dispersion in isotropic turbulence and the influence of the small scales. Of particular concern has been the profile of the structure function $\langle \Delta u^2(r) \rangle$, where Δu is the relative velocity between two fluid elements measured either along or normal to their line of separation and r their distance of separation. The particle collision rate depends upon the flux of particles over the collision boundary surrounding any given particle which in turn depends upon the mean velocity upon impact and the local concentration. As in turbulent boundary layer deposition (Young and Leeming, 1997), there is a peaking of the particle concentration near the collision boundary embodied in measurements of the so-called radial distribution function (RDF) (Sundaram and Collins, 1997) near the collision boundary and an enhancement of impact velocities due to particle inertia referred to as decorrelated velocities (Sundaram and Collins, 1997). In this regard it is revealing to recall the recent work of Zaichik and Simonin (2006) who identified these velocities as the source of random uncorrelated motion (RUM) that has been observed in DNS measurements of the particle velocity field and which forms an important part of the Simonin two-fluid model approach (Fevrier et al., 2005).

Of particular relevance to this study are the recent works of Zaichik and his co worker (Zaichik and Alipchenkov, 2003, 2005, 2006) and Chun et al. (2005) who both used a probabilistic approach to calculate the RDF. Zaichik in particular used a PDF approach analogous to the kinetic theory for which he and others have used in previous studies to generate the mass, momentum and kinetic stress equations of dispersed particles in a turbulent flow (the so-called continuum equations for single particle dispersion) (see, e.g. Reeks and Simonin, 2006). Zaichik recognized that the same kinetic equation could be used to describe the relative dispersion and collision rate of pairs of monodisperse particles with particle velocity (in a fixed frame of reference) replaced by the relative velocity between particle pairs. Thus, if $\underline{v}$ is the relative velocity measured at time t between two identical particles separated by a distance $\underline{r} = [x_i, i = 1, 3]$, the equation for the PDF $P(\underline{v}, \underline{r}, t)$ assuming Stokes drag is

$$\frac{\partial P}{\partial t} + v_i \frac{\partial P}{\partial x_i} - \frac{\partial}{\partial v_i} \beta v_i P = \frac{\partial}{\partial v_i} \beta \langle \Delta u_i p \rangle \tag{1}$$

where $p(\underline{v}, \underline{r}, t)$ is the instantaneous phase space density for a single realization of the carrier flow field, and $\Delta \underline{u}(\underline{r}, t)$ is the relative velocity of the fluid encountered by the two particles with inverse response time β. Agglomeration and relative dispersion is controlled by the small scales of the turbulence. So by exploiting local isotropy of the small scales and assuming spherical or cylindrical symmetry, this equation can be used to calculate the collision rate and RDF.

There are three important features of this PDF approach that are worth noting. The first is the choice of closure for the phase space diffusion current $\beta \langle \Delta u_i p \rangle$, for which Zaichik along with others have assumed a Boussinesq gradient diffusion approximation (Reeks and Simonin, 2006). The second is the handling of the boundary conditions which depend on whether the collision process is partially or perfectly absorbing. This places a restriction on the form of P at the collision boundary and necessitates an explicit solution of the PDF equation. This is in contrast to the traditional approach based on the moment equations of the PDF where the boundary conditions are artificially imposed or where some assumptions on the velocity distribution at the collision boundary are made (e.g. half Gaussian as Zaichik and Alipchenkov (2003) have done). The third is the fundamental basis upon which the RDF is based at equilibrium (perfect reflection at the collision boundary), namely a force balance between the particle kinetic stresses and the net drag due to the relative velocity of the turbulence. So with reference to Eq. (1), equilibrium means explicitly

$$-\nabla \cdot \langle \rho \underline{v} \underline{v} \rangle + \beta \langle \rho \Delta \underline{u} \rangle = 0 \tag{2}$$

where in Zaichik's (2003) PDF approach $\langle \rho \Delta \underline{u} \rangle$ is modeled as a gradient diffusion term involving the particle–fluid diffusion coefficient. Given the problems with dealing with the boundary conditions at the collision boundary, Zaichik's solutions to the moment equations of the PDF equation accurately replicate the important features of both deposition in a turbulent boundary layer and turbulent agglomeration/segregation when compared to DNS solutions.

In contrast, Chun et al. (2005) use a different probabilistic approach applying it to particles with small Stokes numbers, which in essence treats the particles as passive scalars transported by their own velocity field $\underline{v}(\underline{r}, t)$ (in the case of two particle dispersion, it is the relative particle velocity field between particles a distance $\underline{r}$ apart). The collision flux is modeled as the sum of two parts, namely a 'shear' diffusion flux $\underline{q}_D$ which depends on the mean concentration gradient of the satellite particles surrounding a target primary particle and a drift flux $\underline{q}_d$ that depends upon the local mean concentration of satellite particles and the compressibility of the relative particle velocity field. Explicitly for small Stokes numbers, where the concentration gradient is a small perturbation on the uniform concentration for passive tracers,

$$q_i^D = -D_{ij} \frac{\partial \langle \rho \rangle}{\partial r_j}; \quad D_{ij} = \int_{-\infty}^{t} \langle v_i(\underline{r}, t) v_j(\underline{r}', t') \rangle dt' \tag{3}$$

where $\underline{r}'$ is the position of a particle at time t' which arrives at $\underline{r}$ at time t and D_{ij} is the dispersion coefficient for relative dispersion; and

$$q_i^d = -\int_{-\infty}^{t} \langle \underline{v}(\underline{r},t)\nabla_{\underline{r}'}\cdot\underline{v}(\underline{r},t|\underline{r}')\rangle dt' \langle \rho(\underline{r},t)\rangle \quad (4)$$

which explicitly involves the divergence $\nabla_{\underline{r}'}\cdot\underline{v}(\underline{r},t|\underline{r}')$ of the relative particle velocity field along a particle trajectory $\underline{r}'(t')$ which arrives at $\underline{r}$ at time t. We note that the form for the drift flux is the same as the form proposed by Maxey (1987) for the enhancement of drift due to gravity and the form derived by Reeks (2005a) for particle dispersion in an inhomogeneous compressible flow field. In contrast to Eq. (4), the RDF is based on a balance of mass fluxes, namely

$$\underline{q}^d + \underline{q}^D = 0 \quad (5)$$

With the particle velocity field derived from a perturbation expansion in St obtained from the equation of motion of particle pairs transported in a linear carrier flow field.

Expressions for this term show that to first order in St, $\nabla\cdot\underline{v}(\underline{r},t) \sim St(\langle S^2\rangle - \langle R^2\rangle)$, where we recall $\underline{S}$ is the local symmetric strain rate tensor and $\underline{R}$ the local rotation tensor. In isotropic homogeneous flow, $\langle S^2\rangle = \langle R^2\rangle$ for a fluid element, indicating that to first order in St, $\underline{q}_d = 0$, necessitating a higher order expansion $O(St)$ for the difference $\langle S^2\rangle - \langle R^2\rangle$ along a particle trajectory.

It is important to recognize that whilst the two approaches eventually lead to the same form for the dependence of RDF upon St (for $St \ll 1$) in 3D isotropic turbulence, namely $r^{-\alpha St^2}$, the values of the constant α in either case though similar are different reflecting the difference in the way RDF has been derived and the approximations that have been made. In the first case Chun et al. (2005) compressibility plays an explicit role in determining the drift flux, in the second case (Zaichik and Alipchenkov, 2003) it appears only implicitly through its influence on the values of the kinetic stresses being weighted towards regions of high strain rate in the flow. However, in the sense that both approaches involve the particle equation of motion, they should give the same result for $St \ll 1$ providing the same model for the underlying turbulence is used.

Bearing in mind this difference in approach, the work we present here has several things in mind. The first as we have said earlier is to provide a simple model for turbulent agglomeration (and also breakup). With the aid of this model, the second is to examine in more detail the validity of some of the assumptions that are made in the application of more complex approaches, e.g. in the application of DNS itself and in the probabilistic approaches. There are for instance certain assumptions that are made in the application of the classical Saffman and Turner model which we can critically assess with the use of simple models, in particular the fully mixed assumption and the fact that the flow field is assumed to be frozen. Collisions rates with perfect absorption can be significantly different from those with perfect reflection. The role of the persistence or finite life-time of turbulent structures can make particle collision rates very much rate-limited by diffusion as is the case of particle transport in a turbulent boundary layer.

We are mindful of the fact that a number of these features have been examined in detail in previous studies involving DNS and KS models that are similar to the one used here. Wang and his co workers (Wang et al., 1998a,b) have examined the validity of the S&T model for the collision rate of tracer (inertialess) particles focusing on the difference between perfect reflection on collision (particles not removed from the flow after collision) and those where particle pairs adhere after collision (particles removed from the flow after collision). Brunk et al. (1998) examined intensively the response of the agglomeration rate to changes in the correlation time of the velocity gradients in the flow for inertialess particles. We shall have recourse to refer to the results of both these investigations in the course of this study. What we have done here that is different to previous studies is to examine all of these features together. The simplicity of the model gives a greater scope to isolate and control the various parameters in an independent way than would be in using DNS. However, perhaps the most important feature of the work we report here is the way we have analyzed and described the steady state collision flux as arising from a balance of net forces acting on the satellite particles due to surface forces derived from the kinetic stresses, and the net drag force due to the turbulence.

Therefore in what follows, Section 2 recalls the theoretical expressions for the collision kernels in the limit of inertialess particles (S&T model) in the context of the present case which for reasons we explain later is chosen to be 2D to begin with.

Section 3 gives the details of the random symmetric straining model and Section 4 gives the continuum (mass and momentum) equations for the dispersed particles relative to the test particle and shows how they can be expressed alternatively as gradient diffusion versus drift as has been done before in the context of turbulent deposition (Reeks, 2005a). We show how this approach leads to the quasi-local homogeneous (QLH) solution for the collision kernel.

The results of simulation are presented and discussed in Section 5. In particular we examine and discuss the following issues:

1. The dependence of the collision kernel on Stokes number, considering the behavior in the limit of tracer particles ($St \to 0$).
2. The correction to the S&T result for tracer particles due to a change of boundary conditions from perfectly reflecting to perfectly adhering.
3. Identification of the important features that influence turbulent agglomeration, in particular the particle concentration and the particle velocity distribution at the collision boundary and how they depend on Stokes number.
4. How the agglomeration rates can be explained by a competition between diffusive and convective currents.
5. The range of Stokes for the validity of the quasi-local homogeneous form of the collision kernel.

2. Collision kernel for inertialess particles ($St = 0$)

As mentioned in the introduction, S&T determined the collision kernel for inertialess tracer particles of size much smaller than the Kolmogorov length scale. For the case of colliding spherical particles, the flux of tracer particles through the surface of the collision boundary of radius r_c is assumed to be contained in the flux of fresh carrier flow entering the collision boundary j_r^+ (cf. Fig. 1), where j_r^+

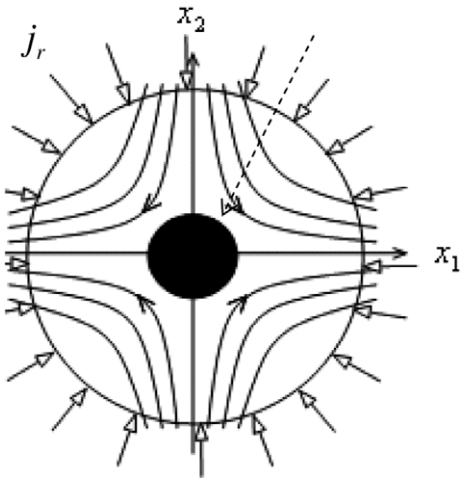

Fig. 1. Location of collision boundary (circle of radius r_c) of two colliding particles at the centre of a symmetric straining flow together with injection circle (radius R) of satellite particles. j_r is the radial current of injected particles at $r = R$ towards the collision boundary.

is the carrier flow volume flux arriving at the surface (per unit area) with + denoting carrier flow moving towards the surface. So if $p(\underline{v}, r_c)$ is the carrier flow phase space density (PDF) for carrier flow velocity $\underline{v}$ at r_c, then

$$j_r^+ = \int v_r^+ p(\underset{\rightarrow}{v}\, r_c) d\underline{v} \tag{6}$$

where v_r^+ is the carrier flow velocity along the radius of the collision boundary pointing towards its surface. S&T assume that the colliding tracer particles have the same velocity distribution as the carrier flow so that the number of particles traveling towards and away from the collision boundary are equal, and in particular $p(v_r, r_c) = p(-v_r, r_c)$. This leads to the result $j_r^+ = \frac{1}{2} n_c \langle |v_r| \rangle$, where j_r^+ is the particle flux (number of colliding particles/unit area/s) moving towards the collision boundary upon collision, n_c is the number density of tracer particles at the collision boundary, and $\langle |v_r| \rangle$ is the average of the absolute value of the tracer particle (carrier flow) radial velocities (for both +ve and −ve radial velocities) at the collision boundary. The factor of 1/2 arises simply because 1/2 the particles are moving towards the collision as are moving away (i.e. this corresponds to a perfectly reflecting boundary condition). For tracer particles in a fully mixed flow where the particles are fully mixed even up to the collision boundary, $n_c = n_\infty$ where n_∞ is the concentration of particles at a distance $r \gg r_c$, where the particles are assumed to be in steady state equilibrium.

The carrier flow field relative to the test particle is assumed to be isotropic and normally distributed with variance $\sigma^2(r)$.

In S&T's work, the mean absolute radial fluid velocity $\langle |v_r| \rangle$ was based on a Gaussian distribution of flow velocities and given explicitly by

$$\langle |v_r| \rangle = \frac{1}{\sqrt{2\pi}\sigma} \int_{-\infty}^{\infty} e^{\frac{v_r^2}{2\sigma^2}} |v_r| dv_r = \sqrt{\frac{2}{\pi}} \sigma(r) \tag{7}$$

The collision kernel is defined as

$\Gamma =$ target area $\times\, j_r^+(r_c)/n_\infty$ and therefore given explicitly in S&T by

$$\Gamma = 2\pi r_c^2 \langle |v_r| \rangle = 2\pi r_c^2 \sqrt{2/\pi}\, \sigma(r_c) \tag{8}$$

with

$$\sigma(r) = \left\langle \left(\frac{\partial u}{\partial x} \right)^2 \right\rangle^{1/2} r \tag{9}$$

and

$$\left\langle \left(\frac{\partial u}{\partial x} \right)^2 \right\rangle = \frac{2\varepsilon}{15\nu} \tag{10}$$

In the present case, a 2D geometry is considered so that the target area is that of a cylinder of radius r_c and therefore Eq. (8) becomes

$$\Gamma = \pi r_c \langle |w_r| \rangle = \left(\frac{4\pi\varepsilon}{15\nu} \right)^{1/2} r_c^2 \tag{11}$$

As noted previously (Wang et al., 1998a,b) S&T obtained this expression for a uniform time independent carrier flow field (i.e. a frozen field).

3. Random symmetric strain model

3.1. Choice of structure for small scale turbulence

We chose the basic structure of a symmetric straining flow to study collisions for historic reasons and for the role it plays in the S&T model for turbulent agglomeration of tracer particles. In using this to represent the motion of the small scales structure, we must take account of the fact that the random flow be isotropic and satisfy the requirement for homogeneity of the turbulent velocity gradient (e.g. Pope, 2000). This means in general that the flow must have equal amounts of straining and rotation. More explicitly if $\underline{S}$ and $\underline{R}$ are the strain rate and rotation tensors, $\langle S^2 \rangle - \langle R^2 \rangle = 0$, where $S^2 = \underline{S}:\underline{S}$, implying that one cannot in general construct a homogeneous flow field from a straining flow field alone. However, we note that this requirement for homogeneity is based on the basic requirement that $\partial/\partial x_i \langle u_j \partial u_i / x_i \rangle = 0$ and the assumptions that the flow is incompressible and that $\partial/\partial x_i$ and $\langle\ \rangle$ commute. In the case of a 2D straining flow composed of step changes in the strain rate as is the case we consider here, the commutation rule does not apply. However, the basic condition for homogeneity is still satisfied. In fact we have confirmed this by constructing a random periodic flow field composed of a sequence of symmetric straining flows back to back and displacing the flow pattern randomly over its periodic length whilst randomly rotating its principal axes (Reeks, 2005a). In 2D for equal amounts of strain and vorticity, the relationship between the variance of the tangential (θ) and radial (r) components should be $\langle u_\theta^2 \rangle = 3\langle u_r^2 \rangle$ whereas for straining only $\langle u_\theta^2 \rangle = \langle u_r^2 \rangle$. We can overcome the problem of the deficit of rotation, by adding to the straining flow a rigid body rotation which would add to the value of the variance of the tangential component without affecting the corresponding value of the radial component. However, we have not done so here, leaving the influence of adding vorticity to the flow as a separate study since this can be done in a number of ways depending on the correlation between the two types of structures (e.g. as free and statistically independent vortices and straining flows or bound up in pairs of counter rotating vortices, etc.). We believe that the use of a simple straining flow field is the most representative structure for considering the segregation for $St \sim 1$ where the agglomeration rate is likely to be greatest, because under these circumstances the particles motion will be biased towards regions of high strain rate rather than vorticity. A pure straining flow is also useful in that it highlights the difference between the two probabilistic methods that have been used to model the radial distribution function (RDF).

It is true that as a starting point, it would have been better to have dealt with a 3D isotropic flow rather than a 2D. Unfortunately whilst we have been able to construct such a flow field in 3D by suitable rotations about the principal axes of the straining flow element, we have been unable to construct from it a flow field that is homogeneous as well. So in the end we focused on the simpler 2D or cylindrical geometry.

3.2. Generating a 2D isotropic straining flow

Isotropic turbulent flow relative to moving test particle is generated by randomization of a symmetric straining flow (see Fig. 2). This flow persists for an eddy life time T selected from an exponential distribution with a decay time constant equal to $\langle \dot{\gamma} \rangle^{-1/2}$. A new 2D flow field is then generated with a new value of T and a new value of the strain rate $\dot{\gamma}$ selected from a Gaussian distribution of variance $\langle \dot{\gamma}^2 \rangle$ and at the same time the principal axes of the flow are rotated by an angle θ selected from a uniform distribution $[0, 2\pi]$ (cf. Fig. 2). The process will generate an isotropic Gaussian straining flow field whose moments depend only on the radial distance from the origin of the straining flow. In particular the RMS velocities in the radial (longitudinal) and polar (lateral) directions are in 2D:

$$\langle v_r^2 \rangle = \langle v_\theta^2 \rangle = \frac{1}{2} \langle \dot{\gamma}^2 r^2 \rangle \tag{12}$$

where r and θ refer to the radial and polar directions, respectively.

The particle equations of motion refer to the principal axes of the straining flow (which rotate depending on the angle θ) and have a simple analytic solution, which is used to construct a final solution in a fixed frame of reference of the particle test located

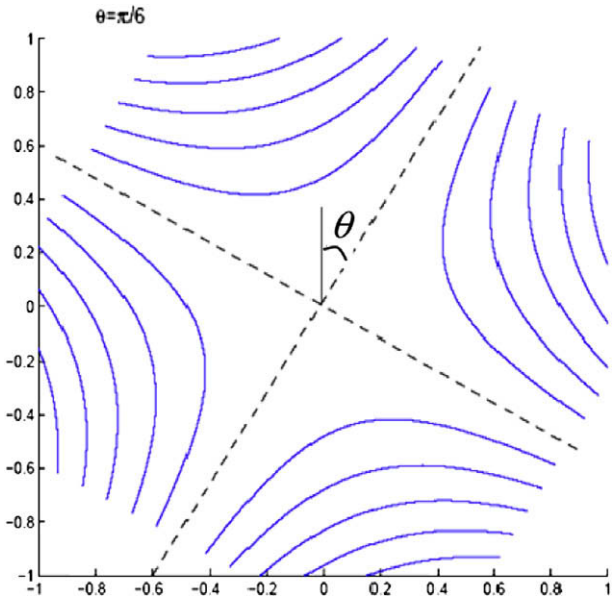

Fig. 2. Rotation of the straining flow by an angle θ.

at the centre of the control volume. This avoids the use of numerical methods and therefore speeds up the simulation. In the particle test frame of reference, the particle velocity will therefore represent the relative velocity between two particles (and in particular two colliding particles).

Within the gas–solid flow approximation, the equation of relative motion of the particles having the some response time reduces to:

$$\ddot{x}_j + \tau_p^{-1}\dot{x}_j - \tau_p^{-1}\dot{\gamma}_j x_j = 0, \quad j,1,2 \tag{13}$$

where $\dot{\gamma}_1 = \dot{\gamma}, \dot{\gamma}_2 = -\dot{\gamma}$, and τ_p is the particle response time.

In this paper only collisions between small monodisperse particles are considered in isotropic turbulence. As in S&T, the size of the particles is assumed to be $\ll$ the Kolmogorov length scale $\eta = (\nu^3/\bar{\varepsilon})^{1/4}$, where ν and $\bar{\varepsilon}$ are the fluid kinematic viscosity and the average rate of energy dissipation per unit mass, respectively. For convenience in what follows we have scaled distances on the Kolmogorov length scale η_K, and times on the inverse rms strain rate $\langle\dot{\gamma}^2\rangle^{-1/2} = \langle(\partial u/\partial x)^2\rangle^{-1/2}$. So in terms of the scaled variables, the S&T result for the collision kernel in these 'normalized' units for a cylindrical geometry is given by

$$\Gamma = \sqrt{\pi r_c^2}. \tag{14}$$

where the collision radius r_c is in units of η.

The equation of motion (13) becomes for j = 1,2:

$$\ddot{x}_j + \frac{1}{St}\dot{x}_j + \frac{\dot{\gamma}_j}{St}\dot{x}_j = 0. \tag{15}$$

$$St = \tau_p\langle\dot{\gamma}\rangle^{1/2}.$$

We note that in this model $\dot{\gamma}$ is a Gaussian random variable of zero mean and unit variance.

3.3. Procedure

3.3.1. Particle injection

To obtain steady state equilibrium, particles are continuously released from the edge of the circular domain with a variable time delay between each release. The time delay is equal to $\eta(2N_P\sigma_P)^{-1}$, where N_p is the number of particles required in the domain to achieve statistical equilibrium and σp is the particle rms velocity.

We assume that outside the circular domain, the carrier flow is homogeneous and stationary and that particles injected into the domain are in equilibrium with this outer flow so that the velocity correlation coefficient between the particles and the carrier flow is

$$\Lambda = \frac{1}{\sqrt{1+St}}. \tag{16}$$

as is also the ratio of particle/fluid rms velocities. To achieve this, we generate at the same time as $\dot{\gamma}$, a strain rate $\dot{\gamma}_p$ selected from a Gaussian distribution of zero mean and unit variance and correlated with the fluid strain rate $\dot{\gamma}$ of the random symmetric straining carrier flow with a correlation coefficient Λ. In particular

$$\dot{\gamma}_p = \Lambda\dot{\gamma} + (1-\Lambda)^{1/2}\dot{\gamma}' \tag{17}$$

where $\dot{\gamma}'$ is selected from the same Gaussian distribution as that of $\dot{\gamma}$ but statistically independent of it. The particle injection point is chosen randomly around the edge of the circular domain by selecting its angular location from a uniform distribution $U[0, 2, \pi]$, the injected particles being given a velocity

$$\underline{v}_p(\underline{x}) = (\Lambda\dot{\gamma}_p x_1, -\Lambda\dot{\gamma}_p x_2) \tag{18}$$

Subsequently a second particle is injected with a velocity defined by choosing a second value of the strain rate $\dot{\gamma}_p$ but keeping the same value of the strain rate of the carrier velocity field until the lifetime of the fluid straining flow exceeds the eddy lifetime T.

3.3.2. Boundary condition

As particles approach each other to within a diameter or so they begin to influence each other's motion by disturbance of the intervening flow. The relative motion is affected and if one particle is smaller than the other then it can follow the streamline around the other particle rather than collide. Thus, the actual collision frequency is reduced by a factor equal to the collision efficiency. In this study the collision efficiency is assumed to be unity and therefore all the collisions result in agglomeration of the particles. Numerically this is reflected in the choice of the boundary condition at the collision boundary. The particles are tracked until they collide. After collision they are removed from the domain and the boundary condition is said to be perfectly absorbing.

3.3.3. Quasi steady state behavior

Particles are distributed uniformly in the domain at time t = 0 and are then injected at random initial positions at the edge, one after the other with a constant rate proportional to the inverse of the required number of particles in the domain following the procedure described above for their initial velocities.

Fig. 3 depicts the fluctuations of the number of particles in the domain as a function of time and the Stokes number. The sampling time should be long enough to count sufficient number particles and small enough compared with the interval of time to reach steady state.

The equation for the conservation of mass/particle number is given by:

$$\frac{\partial\langle\rho\rangle}{\partial t} = \frac{1}{r}\frac{\partial}{\partial r}rj_r \tag{19}$$

where $j_r = \langle\rho v_r\rangle$ is the radial current. $\rho(r)$ is defined to be the instantaneous radial number concentration of particles at a distance r from the centre of any individual particle (all particles being identical with one another).

At equilibrium $\frac{\partial\langle\rho\rangle}{\partial t} = 0$ and Eq. (19) reduces to

$$rj_r = C \tag{20}$$

where C is a constant.

Fig. 4 shows that according to Eq. (19) the steady state is reached. Fig. 5 depicting the trend of the concentration measured

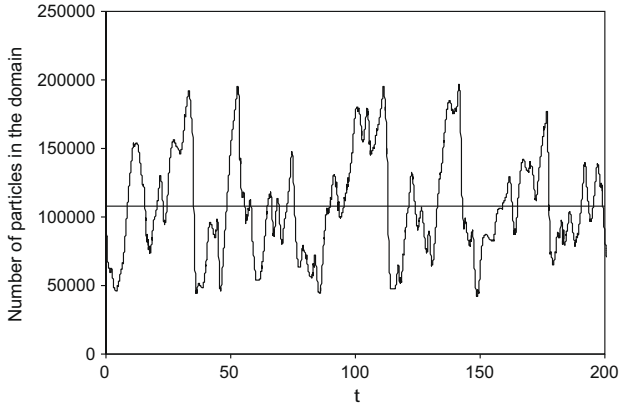

Fig. 3. Number of particle in the domain versus time ($St = 1$).

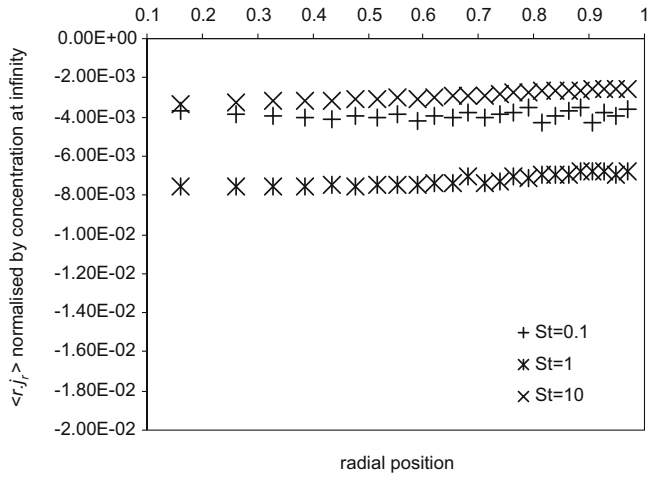

Fig. 4. Conservation of mass at steady state for injection circle at radial position $r = 1$ and collision radius $r_c = 0.1$.

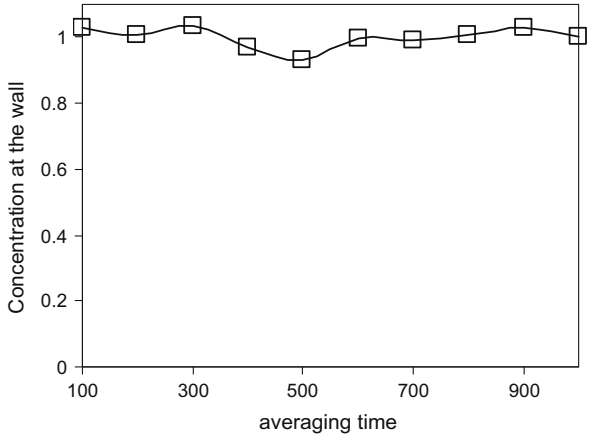

Fig. 5. Concentration at the collision boundary as a function of the averaging time for $St = 0.1$ and $r_c = 0.1$.

at the collision radius as a function of the averaging time confirms equilibrium behavior for the statistics at collision.

Once equilibrium is reached, the particle average flux and concentration are calculated by averaging over a large period of time for all the particles in domain flow and the flux of colliding particles is measured by counting the number of particles striking the collision circle. Averaging is performed when equilibrium in particle concentration is obtained, the flow field containing a sufficiently large number of particles to achieve statistical stationarity. Typically 10^5 particles are required in the domain to achieve good statistics.

4. The mass and momentum equations

The straining flow extends to a radius $R \approx 1$. Beyond R we assume particles are fully mixed, this region forming a region of homogeneous turbulence in which the particles are in equilibrium. In the context of S&T's work, $r_c/R \ll 1$.

The continuity equation for mass at equilibrium is given by Eq. (20) where the constant C can be written as a function of the collision kernel such as:

$$rj_r = r\langle \rho v_r \rangle = C = -\Gamma\langle \rho(R)\rangle/(2\pi) = -KR\langle \rho(R)\rangle \tag{21}$$

The particles are assumed fully mixed outside the injection circle and therefore $\langle \rho(\infty)\rangle = \langle \rho(R)\rangle$.

k = mass transfer coefficient so that $\Gamma = 2\pi RK$. For convenience the concentration is scaled on $\langle \rho(R)\rangle$ which is equivalent to setting $\rho(R) = 1$ so that Eq. (21) reduces to

$$rj_r = r\langle \rho v_r \rangle = C = -\Gamma/(2\pi) = -kR \tag{22}$$

Hence, particles arrive at this target area under steady state conditions so that the net concentration of particles is constant in time corresponding to a constant net flux at any position r. Furthermore, the net current is independent of its tangential coordinate being in the $-$ve r direction. Assuming equilibrium, the averaged momentum equation for the particles will be

$$\nabla \cdot \langle \rho \mathbf{vv} \rangle = St^{-1}(\langle \rho \mathbf{u} \rangle - \langle \rho \rangle \bar{\mathbf{v}}) \tag{23}$$

With $(^-)$ meaning density weighted average.

In terms of $(r, v_r, \theta, v_\theta)$ and noting that

$$\nabla \cdot \mathbf{v} = r^{-1}\left(\frac{\partial}{\partial r} r v_r + \frac{\partial v_\theta}{\partial \theta}\right) \tag{24}$$

the LHS of Eq. (23) becomes

$$\begin{aligned} \nabla \cdot \langle \rho \mathbf{vv} \rangle &= r^{-1}\left\langle \left(\frac{\partial}{\partial r}\rho r v_r + \frac{\partial \rho v_\theta}{\partial \theta}\right)(v_r \hat{\mathbf{r}} + v_\theta \hat{\boldsymbol{\theta}}) \right\rangle \\ &= \left(\frac{\partial \langle \rho v_r^2 \rangle}{\partial r} + \frac{\langle \rho v_r^2 \rangle - \langle \rho v_\theta^2 \rangle}{r}\right)\hat{\mathbf{r}} - \frac{\langle \rho v_r v_\theta \rangle}{r}\hat{\boldsymbol{\theta}} \end{aligned} \tag{25}$$

where a polar angle θ independence of all averaged quantities is assumed. The last term (the average Coriolis force) is zero because the random shear flow is isotropic. Thus, the particle momentum equation in the radial direction becomes

$$-\frac{1}{r}\frac{d\langle \rho r v_r^2 \rangle}{dr} + \frac{\langle \rho v_\theta^2 \rangle}{r} + St^{-1}\langle \rho u_r \rangle - St^{-1}\langle \rho \rangle \overline{v_r} = 0 \tag{26}$$

$\frac{1}{r}\frac{d\langle \rho r v_r^2 \rangle}{dr}$ is derived from the net force (per unit volume) of the radial kinetic stresses, $\frac{\langle \rho v_\theta^2 \rangle}{r}$ represents the centrifugal force and $St^{-1}\langle \rho u_r \rangle - St^{-1}\langle \rho \rangle \overline{v_r}$ is the Stokes drag. The radial kinetic stress contribution provides a direct pressure term $-\frac{\langle \rho v_r^2 \rangle}{r}$ which counteracts the centrifugal force and a radial gradient of the kinetic stresses. Recognizing this feature, and for future analysis, we rewrite the radial momentum equation in a form that shows the contribution that these forces (per unit volume) make to the radial current j_r, namely

$$\begin{aligned} j_r &= \langle \rho \rangle \overline{v_r} \\ &= \langle \rho u_r \rangle + \left(\overbrace{-St\frac{d\langle \rho v_r^2 \rangle}{dr}}^{\text{gradient of kinetic stresses}} + \underbrace{St\frac{\langle \rho v_\theta^2 \rangle - \langle \rho v_r^2 \rangle}{r}}_{\text{net centrifugal force}} \right) \end{aligned} \tag{27}$$

4.1. The momentum equation as a convection–diffusion equation

The momentum equation can be can be further expressed as a convection–diffusion equation by expressing the gradient of the radial kinetic stresses in Eq. (27) in terms of a convective force (depending only on the particle concentration) and a diffusive force (depending on the concentration gradient and higher order derivatives of the concentration), thus Eq. (27) becomes

$$j_r = \underbrace{\langle\rho\rangle\left[-St\frac{\partial\overline{v_r^2}}{\partial r}+St\left(\frac{\overline{v_\theta^2}-\overline{v_r^2}}{r}\right)\right]}_{convective}+\underbrace{\left[\langle\rho u_r\rangle-St\overline{v_r^2}\frac{\partial\langle\rho\rangle}{\partial r}\right]}_{diffusive} \tag{28}$$

The first term on the RHS is a convection current and the second term a diffusive current. The convection current arises from a drift velocity made up of: (1) a turbophoretic drift $-St\frac{\partial\overline{v_r^2}}{\partial r}$ (towards the collision boundary); (2) a net centrifugal drift $St\left(\frac{\overline{v_\theta^2}-\overline{v_r^2}}{r}\right)$ away from the collision boundary whereas $j_d=\left[\langle\rho u_r\rangle-St\overline{v_r^2}\frac{\partial\langle\rho\rangle}{\partial r}\right]$ represents the diffusive current. We suppose that $\langle\rho u_r\rangle$ depends only on the gradient of the mean particle concentration so that we can write the diffusive current $j_d=\left[\langle\rho u_r\rangle-St\overline{v_r^2}\frac{\partial\langle\rho\rangle}{\partial r}\right]$ as

$$J_d=-\varepsilon_p\frac{d\langle\rho\rangle}{d\tilde{r}} \tag{29}$$

with

$$\varepsilon_p=\varepsilon_{fp}+St\overline{v_r^2} \tag{30}$$

with $\varepsilon_{fp}=-\frac{\langle\rho u_r\rangle}{(d\langle\rho\rangle/dr)}$

ε_{fp} has been referred to as the fluid particle diffusion coefficient (Simonin, 1996). In homogeneous flow, it is given by $\varepsilon_{fp}=\langle\Delta r(r,t|0)u_r(r,r)\rangle$, Eq. (30) defining a fundamental relationship between this diffusion coefficient and the particle diffusion coefficient involving an inertial contribution $St\overline{v_r^2}$ (see the inertial diffusion coefficient introduced by Liu and Ilori to describe inertial/eddy impaction deposition (Liu and Ilori, 1974). Both contributions have a Stokes number (inertial dependence) but their sum (the particle diffusion coefficient) is explicitly Stokes number independent. More precisely in homogeneous stationary turbulence

$$\begin{aligned}St\overline{v_r^2}&=\int_0^\infty e^{-s/St}\langle u(0)u(s)\rangle ds;\\ \varepsilon_{fp}&=\int_0^\infty(1-e^{-s/St})\langle u(0)u(s)\rangle ds\end{aligned} \tag{31}$$

So that

$$\varepsilon_p=\int_0^\infty\langle u(0)u(s)\rangle ds \tag{32}$$

We can write this as $\varepsilon_p=\langle u^2\rangle T_L$ where T_L is the integral timescale of the fluid along a particle trajectory. If we assume that the value of $\varepsilon_p(r)$ in our random symmetric shear flow is based on quasi-local homogenous flow then in dimensionless variables, $\varepsilon_p=\frac{1}{2}T_Lr^2$, where T_L is the ratio of the timescale of the Lagrangian timescale/Eulerian timescale along a particle trajectory. However, it is worth pointing out that in homogeneous turbulence ε_p is a constant equivalent to a material property of the underlying statistics of the particle velocity field. In general it is itself a function of higher order concentration gradients (>1) and so a function of the concentration profile and the boundary conditions we impose (perfectly or partially absorbing).

4.2. Quasi-local homogeneous (QLH) solution ($St \ll 1$)

4.2.1. Description

By assuming quasi-local homogeneous equilibrium, Eq. (27) becomes

$$J_r=-\varepsilon_p\frac{d\langle\rho\rangle}{dr}+\langle\rho\rangle v_T \tag{33}$$

We set $T_L=1$ to be consistent with the simulation so that

$$\varepsilon_p=\frac{1}{2}r^2 \tag{34}$$

where v_T is the turbophoretic velocity arising in this instance from the gradient of the particle kinetic stresses. The net centrifugal drift will be zero for QLH conditions. Specifically

$$v_T=-St\frac{d\overline{v_r^2}}{dr} \tag{35}$$

where the particle mean square velocity $\overline{v_r^2}$ is assumed to be isotropic and for an exponential decaying fluid velocity correlation as in the simulation it is given by

$$\overline{v_r^2}=\frac{r^2}{2(1+St)}. \tag{36}$$

By using Eq. (34) and Eq. (35) in Eq. (33), the equation for the mass transfer coefficient is obtained, namely:

$$kR=\frac{r^3}{2}\frac{d\langle\rho\rangle}{dr}+mr\langle\rho\rangle. \tag{37}$$

with $m=\frac{St}{St+1}$

At the collision radius the boundary condition is perfectly absorbing with a mean radial velocity v_c so that in addition to solution of Eq. (37) for $\rho(r_c)$, we also have:

$$r_c\rho(r_c)v_c=kR \tag{38}$$

Using the solutions for $\rho(r_c)$ in Eqs. (37) and (38), $\rho(r_c)$ can be eliminated and the equation for k is obtained. To complete the solution, we need an expression for v_c in terms of $\overline{v_r^2}$ for perfect absorption. We base this on the assumption that the distribution of particle relative velocities at collision is a half Gaussian, in which case:

$$v_c=\sqrt{\frac{2}{\pi}}(\overline{v_r^2})^{1/2}=\frac{r_c}{\sqrt{\pi(1+St)}} \tag{39}$$

The solution of Eq. (35) is

$$\rho(r)=\left(\frac{R}{r}\right)^{2m}+\frac{k}{(1-m)R}\left(\left(\frac{R}{r}\right)^{2m}-\left(\frac{R}{r}\right)^{2}\right) \tag{40}$$

Substituting this expression for $\rho(r_c)$ in Eq. (40) gives

$$kR=\frac{r_c^2}{\sqrt{\pi(1+St)}}\left[\left(\frac{R}{r_c}\right)^{2m}+\frac{k}{(m-1)R}\left(\left(\frac{R}{r_c}\right)^{2}-\left(\frac{R}{r_c}\right)^{2m}\right)\right] \tag{41}$$

and eventually the expression for k is:

$$k=\frac{R\left(\frac{r_c}{R}\right)^{2(1-m)}}{\sqrt{\pi(1+St)}+(1-m)^{-1}\left(1-\left(\frac{r_c}{R}\right)^{2(1-m)}\right)} \tag{42}$$

Figs. 6–8 give the QLH solution for the collision kernel and the concentration profiles. The build-up of concentration near to the collision boundary is well reproduced with this simple model.

4.2.2. Fluid point, St = 0 case

Putting $St = 0$ in Eq. (41) gives

$$kR=\frac{r_c^2}{\sqrt{\pi}+\left(1-\left(\frac{r_c}{R}\right)^2\right)}. \tag{43}$$

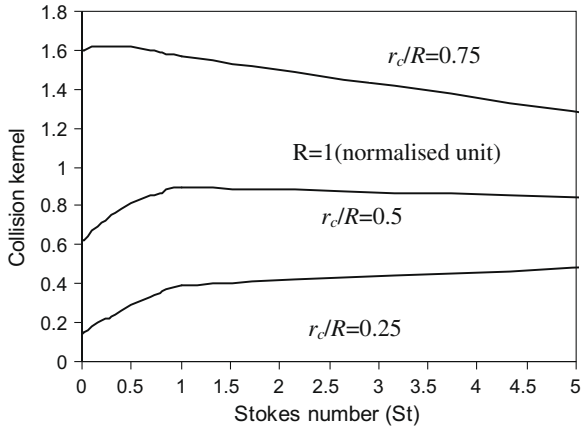

Fig. 6. Collision kernel given by QLH solution versus Stokes number.

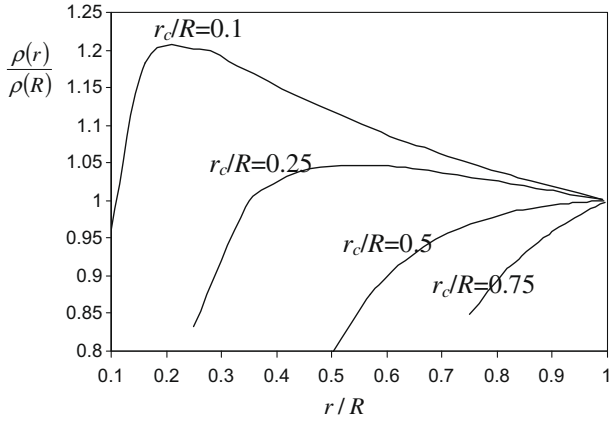

Fig. 7. QLH approximation: concentration profile versus radial position – influence of r_d/R.

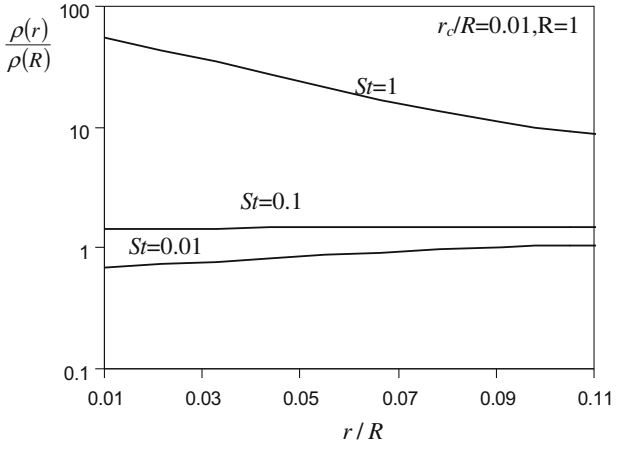

Fig. 8. QLH approximation: concentration profile versus radial position – the influence of the Stokes number *St*.

Implying that the collision kernel Γ is given by

$$\Gamma = 2\pi kR = \frac{2\pi r_c^2}{\sqrt{\pi} + \left(1 - \left(\frac{r_c}{R}\right)^2\right)} \tag{44}$$

so for $r_d/R \ll 1$

$$\Gamma = \frac{2\pi r_c^2}{1 + \sqrt{\pi}} \tag{45}$$

to be compared with the Saffman and Turner fully mixed value

$$\Gamma_{ST} = r_c^2\sqrt{\pi} \tag{46}$$

for a cylinder. This difference is reflected in the concentration at $r = r_c$ given by Eq. (40) for $St = 0$ and $r_c \ll R$

$$\rho(r_c) = \frac{\sqrt{\pi}}{\sqrt{\pi}+1} \approx 0.63909 \tag{47}$$

whereas for S&T $\rho(r_c) = 1$. However, we recall that the actual depositing flux is based on the assumption that this is derived from 1/2 the concentration at the collision boundary. So when comparing agglomeration rates we should compare the value in Eq. (47) with 1/2. Hence the slightly smaller value for the agglomeration kernel based on the Saffman formula than that based on QLH, more precisely

$$\Gamma_{ST}/\Gamma_{QLH} = 0.5/0.63909 = 0.7821.$$

5. Results and discussion

The range of Stokes number chosen in the computation and assessment of the model was between 0 and 10 to cover the two limiting behaviors of small and heavy particles. The results show that this simple model replicates the important features of turbulent agglomeration due to particle inertia that have been observed in DNS as well as giving insight into the influence of perfectly absorbing boundary conditions as opposed to perfectly reflecting.

5.1. Important features of turbulent agglomeration

5.1.1. Relative particle velocity distribution

The particles are injected in the domain with a distribution whose RMS is scaled down by Λ given by Eq. (13) for homogeneous turbulence at equilibrium so that the variance of the distribution decreases as the Stokes number increases near the injection line (cf. Fig. 9). Note that we control only the distribution of velocities of particles injected in the radial direction towards the collision circle which we have made 1/2 Gaussian. Those particles which are traveling away from the collision circle at the injection are determined by their interactions with the random shear and the boundary conditions at the collision circle. At the injection point the overall distribution is close to Gaussian for all the Stokes number cases with the mean velocity $\ll$ particle rms velocity. From Fig. 10, it is noticeable that the distribution for v_θ is very different from the distribution for v_r and in particular the case for $St = 0.1$ reveals that it can be very far from Gaussian even for small Stokes number. The asymmetry suggests a negative skewness.

As far as the distribution for v_r is concerned it is symmetric near the injection line but as particles get closer to the collision

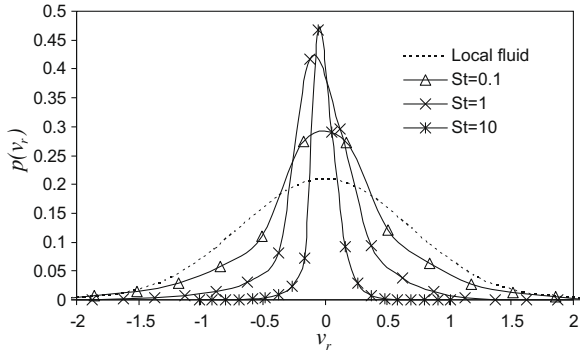

Fig. 9. Particle radial velocity distribution in the shell near the injection circle $R = 1$.

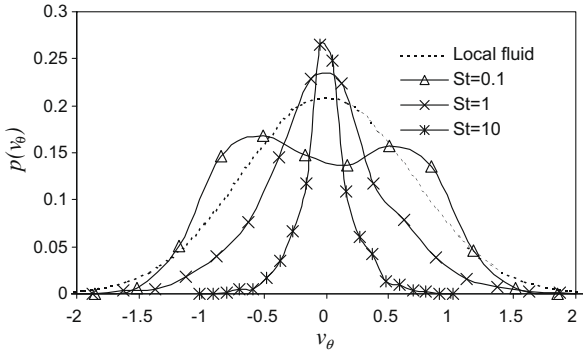

Fig. 10. Particle azimuthal velocity distribution in the shell near the injection circle.

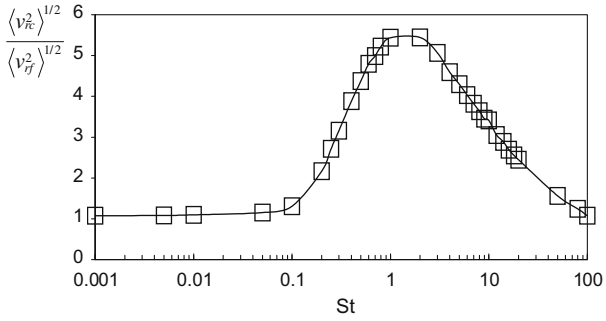

Fig. 13. Ratio of the RMS of the particle velocity distribution at collision boundary over the RMS of the fluid velocity distribution.

boundary the particle relative velocity distribution shifts to velocities directed towards the collision surface (−ve radial velocities) (cf. Fig. 11) and the variance of the distribution diminishes. Note from Fig. 12 that the particle velocity distribution at the collision boundary is significantly different from the half Gaussian assumption made in the evaluation of the agglomeration kernel in the QLH approximation (and used in other approximations). Fig. 13 gives the ratio of the RMS of the velocity distribution of particles at the collision boundary to that of the local carrier flow as a function of Stokes number. The RMS of the particle velocity is equal to the RMS of the fluid velocity for $St \leqslant 0.1$. The curve has got a maximum around $St = 1$ and shows the influence of over shoot for $St < 1$ so that the ratio increases with increasing Stokes numbers instead of decreasing as in the QLH approximation

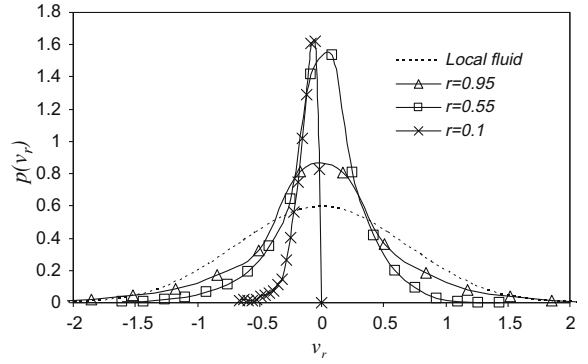

Fig. 11. Comparison of the particle velocity in the shell near the injection circle ($R = 0.95$), in the shell at $r = 0.55$ and at the collision boundary ($r_c = 0.1$) for $St = 0.1$. Note that the negative velocities are toward the collision boundary.

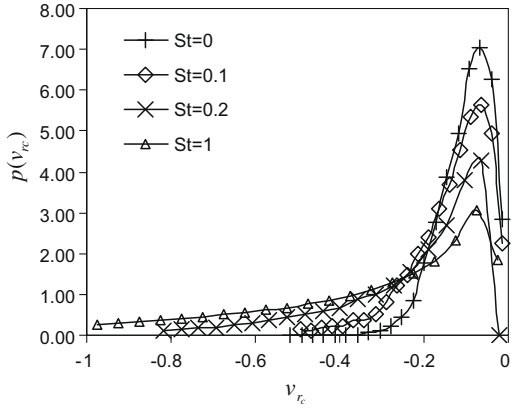

Fig. 12. Particle velocity distribution at the collision boundary for different Stokes numbers, *St*.

5.1.2. Preferential concentration/segregation phenomenon

As observed in DNS simulations (Sundaram and Collins, 1997) a slight build-up of the concentration is observed near the collision boundary for intermediate Stokes number whereas the concentration is largely peaking at the injection line and decreases continuously as it approaches the collision boundary for $St = 0$ and $St = 10$ (cf. Fig. 14).

Note that a reduction in concentration at the collision boundary when it was perfectly absorbing was also observed by Reade and Collins (2000) during their simulation of agglomeration in DNS isotropic turbulence (see Fig. 5 of Reade and Collins 2000). Fig. 15 shows the influence of collision radius on the concentration of tracer (inertialess) particles. The thickness of the concentration boundary layer increases with increasing r_c with a corresponding drop of the concentration at the collision boundary that decreases. The smaller the collision radius the smaller the thickness of the boundary layer, reaching a threshold value at the collision boundary ~ 0.19 for r_c less than 0.1. The range of values of $r_c/R \ll 1$ implies a dependence of the concentration on the ratio r/r_c independent of R which was found to be the case here. In the case of the simple gradient diffusion model proposed in Section 5.2 $\rho(r)$ varies in fact as $(r_c/r)^2$. Note that in all cases considered there is a relatively sharp change in the concentration near or around the

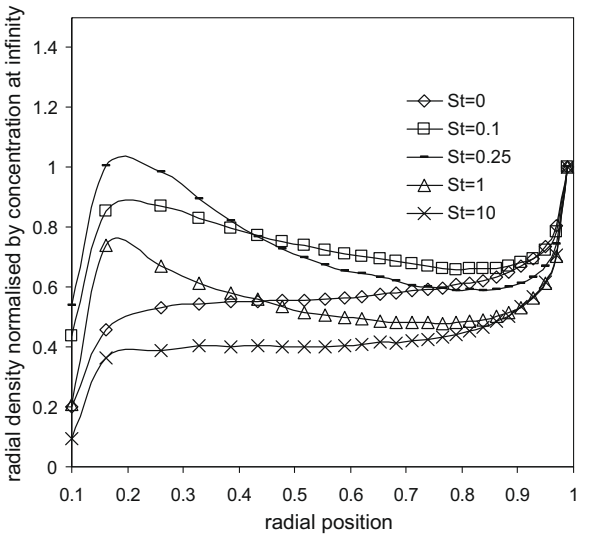

Fig. 14. Radial density normalized by the radial density at injection line ($r = 1$) for different Stokes numbers, *St*.

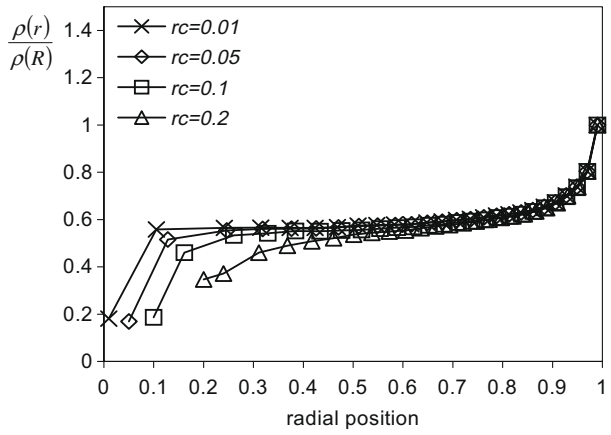

Fig. 15. Radial concentration normalized by radial density at injection line ($r = 1$) versus radial position for inertialess (tracer) particles ($St = 0$).

particle injection point ($r > 0.75$). This region is more pronounced for inertial particles (see Fig. 14). This feature referred to as an 'entrance effect' is common in sprays. Moving the injection point further back will in principle reduce the extent of this region. We shall have need to refer to this region later on when discuss the various contributions to the momentum balance and the influence of absorbing boundary conditions on the collision kernel since this effect is linked to the contribution from the centrifugal force. The asymmetry of the tangential velocity distribution observed in Fig. 10 with a negative skewness reveals that in the shell near the injection line $\langle v_\theta^2 \rangle$ is greater than $\langle v_r^2 \rangle$. As underlined previously this is the consequence of the fact that whilst particles are injected in the domain such as $\langle v_r^2 \rangle = \langle v_\theta^2 \rangle$, there is no control on the particles traveling away from the collision boundary.

5.1.3. Boundary condition

The decrease in concentration at the collision boundary observed in Fig. 14 is influenced by the fact that the collision boundary has been made perfectly absorbing. This is illustrated more graphically in Fig. 16 where we compare the concentration profiles for both perfectly and absorbing boundary conditions for tracer particles ($St = 0$) and particles with $St = 1$. The tracer particles remain perfectly mixed for the perfectly reflecting case, but show a significant drop in concentration ~80% at the collision boundary for perfect absorption. Both boundary conditions show a build-up of concentration near the collision boundary for $St = 1$, though it is more pronounced for perfectly reflecting conditions. The results illustrate the potential error in using the S&T assumptions of perfect reflection conditions to evaluate the agglomeration kernel (equivalent to using a factor of 1/2 for the collision boundary concentration).

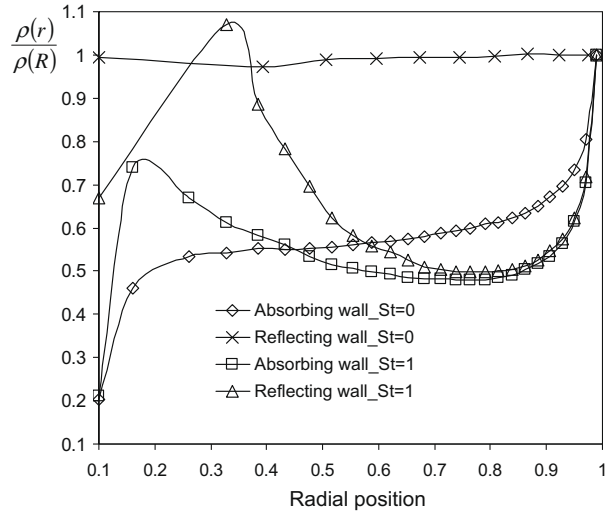

Fig. 16. Radial density normalized by the radial density at injection circle ($r = 1$) versus radial position: comparison of the case for reflection with that for absorbtion at the collision boundary.

Fig. 17 shows the influence of eddy life time T on the concentration profile and in particular upon the concentration of colliding particles at the collision boundary. In particular Fig. 17a shows that the build-up in concentration decreases as the eddy time increases reaching a limiting profile for the frozen field ($T \to \infty$) (the S&T case). In contrast increasing T has no significant effect on the concentration profile for zero Stokes number (Fig. 17b). Similarly increasing T increases the concentration at the collision boundary (Fig. 17c) for $St \sim 0.1$ but has only a relatively small influence (<10%) on the concentration at the collision boundary for inertialess particles. We compare this with a reduction ~20% in the collision kernel compared with the frozen field case (persistent strain rates) which is due mostly (if not all) to the lowering of the concentration at the collision boundary. It is interesting to compare these results for the collision kernel with those of the DNS measurements of Wang et al. (1998a) of the collision kernel in isotropic homogeneous turbulence and those of the simulations in a randomized linear straining isotropic flow of Brunk et al. (1998). The objective in either case was to investigate the dependence of the collision rate upon the boundary condition (whether overlapping (colliding particles) were removed form the system or allowed to continue) and to compare the results with the S&T predictions (appropriate for a frozen field with overlapping particles) using the measured values of $|v_r|$. In our simulation the S&T result is compatible with a uniform concentration (fully mixed flow) arising from perfect reflection at the collision boundary (see Fig. 16). For a perfectly absorbing collision boundary, Brunk et al. (1998) performed a detailed simulation of the influence of timescale of the straining flow on the collision kernel for a range of values of the normalized persistence time T (in units of the inverse rms strain rate). For persistent strains ($T \to \infty$) the collision kernel approached a value which is about 95% of Γ_S (the S&T value) and for $T = 1$, it was ~60% of Γ_S consistent with the values we obtain. In our simulation, increasing the value of T did not have a marked increase on the concentration at the collision boundary for the range of values of $1 < T < 30$. This is consistent with Brunk et al.'s (1998) simulation which showed a similar insensitivity to changes in T, the collision kernel approaching the long time value only when $T \sim 10^3$. Wang et al.'s (1998a) data also indicated a reduced value for the collision kernel compared to Γ_S when the collision boundary is perfectly absorbing in the case a frozen field $\sim 0.85\Gamma_S$. However, in contrast to our results and that of Brunk et al. (1998), Wang et al. (1998a) found that in the case of an evolving field the value of the collision kernel is closer to the S&T value ($\sim 0.9\Gamma_S$). The difference as pointed out by Brunk et al. (1998) is due to the fact that the concentrations of particles in Wang et al.'s simulation do not satisfy conditions of a well-mixed suspension and in the absence of a model for microscale mixing, cannot be compared with either the results presented here or that of Brunk et al. (1998).

5.2. Steady state momentum budget

Figs. 18–20 show the contributions to the radial current j_r towards the collision boundary situated at $r_c = 0.1$ as given in Eq. (27) for $St = 0.1$, 1, 10. We note that for small Stokes numbers ($St = 0.1$) the net centrifugal force is practically zero for $r < 0.75$,

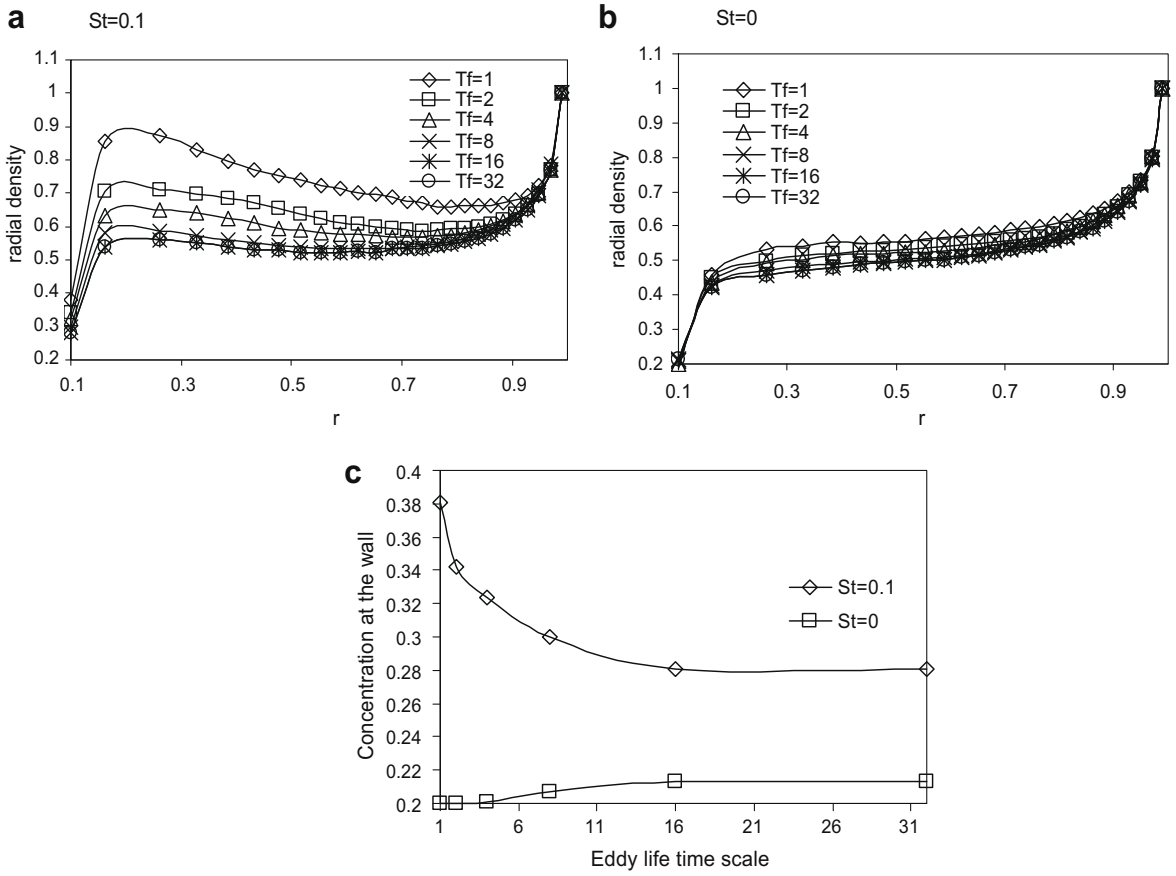

Fig. 17. Radial density normalized by the radial density at injection line ($r = 1$) versus radial position for different eddy life times for $St = 0.1$ (a) and $St = 0$ (b), concentration at the collision boundary versus eddy life time scale (c).

so that the major contribution in this region comes from the diffusive term $\langle \rho u_r$ and the −ve gradient of the radial kinetic stresses $-d/d\langle v_r^2\rangle$ (which is notably −ve and linear in r throughout the whole flow domain). In the region near the collision boundary where the concentration is rising to a maximum (see Fig. 14), the contributions from these two fluxes are of the same sign and both add to the total flux converging towards the same value. Beyond the maximum concentration, the two fluxes are of opposite sign. Both behaviors are consistent with the behavior predicted by the QLH approximation (namely a balance between turbophoretic drift and gradient diffusion). In the region $r > 0.75$, (where the concentration is rising, see Fig. 14), the increasing contribution from the net centrifugal force $\langle \rho \rangle St\left(\frac{\overline{v_\theta^2}-\overline{v_r^2}}{r}\right)$ compensates for the reduction in the diffusive term $\langle \rho u_r \rangle$. However, it noticeable that for +ve concentration gradient in this region, the +ve sign of $\langle \rho u_r \rangle$ is the opposite of that given by simple gradient diffusion (such features as this have been observed before in simple straining flows, suggesting a −ve diffusion coefficient) (Reeks 2005b).

For $St \sim 1$, the contribution from the net centrifugal drift force increases for $r > 0.75$ but also for $r < 0.3$ whilst the diffusion term

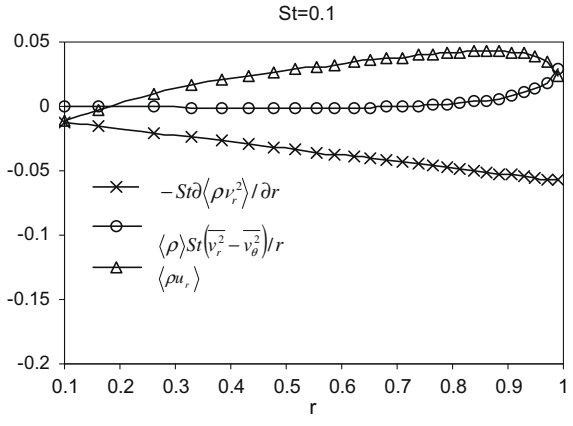

Fig. 18. Terms contributing to the total radial current for $St = 0.1$.

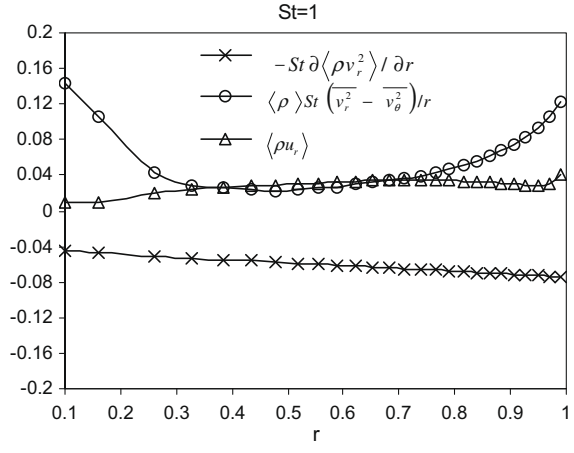

Fig. 19. Terms contributing to the total radial current for $St = 1$.

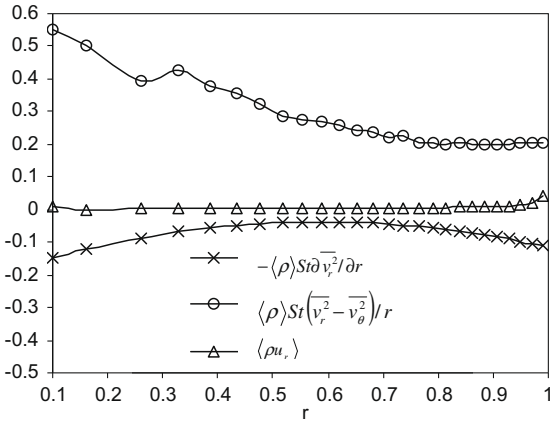

Fig. 20. Terms contributing to the total radial current for $St = 10$.

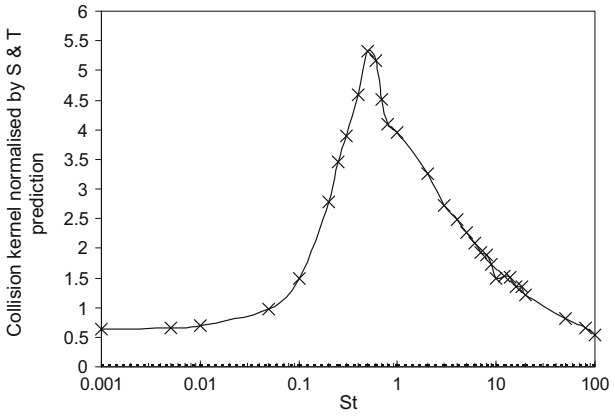

Fig. 22. Collision kernel normalized by S&T prediction versus Stokes number, *St*.

has zero contribution in these two regions. This results in reducing the build-up in concentration at the collision boundary. The turbophoresis presents a linear profile as for the smaller Stokes number. For very large particles ($St = 10$) the diffusive term $\langle\rho u_r\rangle$ becomes negligible for all r and the competition occurs between the net centrifugal drift and the turbophoretic drift.

In order to eliminate the spurious effect induced by the injection, the collision kernel presented in the next section is normalized by the value of the concentration at $r = 0.7$ for comparison with S&T predictions.

5.3. Collision kernel

Fig. 21 shows how the simulated collision kernel for inertialess particles compares with the S&T result in Eq. (27) as the collision radius is varied. But for the lowest value of $r_c = 0.05$ it is more than 1.5 times the S&T prediction due to the perfectly absorbing collision boundary and the consequent lowering of the concentration at the collision boundary compared to its fully mixed value when the collision boundary is perfectly reflecting. For larger collision radii the drop in concentration is less important and therefore S&T becomes acceptable, the drop in concentration at the collision boundary being proportional to the collision radius.

The collision kernel peaks around $St \sim 0.5$ consistent with DNS results but for very large values of St the collision kernel collapses to very small values less than the fully mixed perfectly reflecting value based on S&T values (cf. Fig. 22). We have seen previously that the segregation effect observed in Fig. 14 plays an important role in explaining the peaking of the collision kernel versus *St* in Fig. 22. However, as Sundaram and Collins (1997) pointed out originally it is not the only reason for the peak. Indeed in contrast to the maximum build-up of the concentration at the collision boundary taking place at $St = 0.25$ (the value of *St* for the critically damped oscillations of individual particles), the maximum value of the collision kernel is reached at $St \sim 0.5$. As Sundaram and Collins (1997) have also noted the collision rate depends upon the distribution of impact velocities as well as the local concentration of colliding particles, i.e. the dependence of the collision kernel upon *St* is reflected in the *St* dependence of the particle relative velocity distributions at the collision boundary and in particular upon its variance. Sundaram and Collins (1997) related the variance of the relative velocity to the degree of correlation between neighboring particles as:

$$\overline{v^2} = 2\overline{v_p^2}(1-\chi)) \tag{48}$$

where $\overline{v_p^2}$ is the variance of the velocities of individual particles in a fixed frame of reference and χ is the covariance coefficient defined as $\chi = \frac{\overline{v_1 \cdot v_2}}{\overline{v_p^2}}$ with $0 \leqslant \chi \leqslant 1$ for non-interacting particles. The larger χ the stronger colliding particles are correlated. Thus, the increase in the variance of the particle relative velocity is related to the decrease in correlation of the colliding particles which in turn is caused by a decrease in the correlation of the colliding particles with the local fluid surrounding them. However, decorrelation with the local fluid (which increases the impact velocities) is accompanied with a decrease in the value of $\overline{v_p^2}$, which would also give rise to a peaking of the collision kernel. Therefore, both segregation (Fig. 14) and the particle relative velocity upon impact (Fig. 13) and their dependence on St contribute to the peaking of the collision kernel at $St = 0.5$.

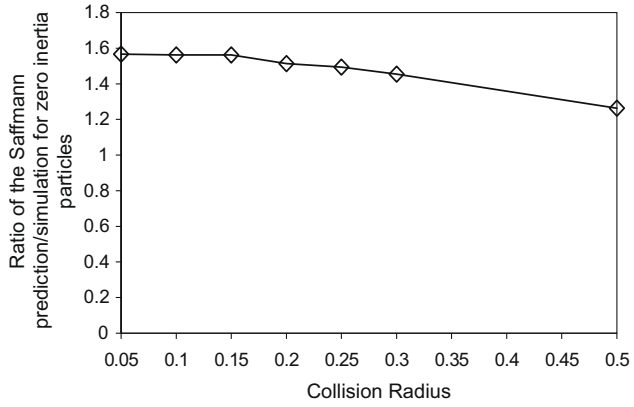

Fig. 21. Ratio of Saffman and Turner prediction over simulated kernel for inertialess (tracer) particles ($St = 0$).

5.4. Validity of the QLH approximation for the prediction of the turbulent collision kernel

The simulation and the QLH solutions for the collision kernel agree well for $St < 0.5$ (cf. Fig. 23). Beyond this range the QLH predictions are consistently much greater than the simulations values which show a peaking at $St \sim 0.5$ and a gradual reduction beyond this value. We recall from Fig. 19 that the collision flux near the collision boundary is dominated by the influence of the net centrifugal force which leads to a reduction of both the concentration and impact velocities at the collision boundary. In contrast there is a significant build-up of concentration near the collision boundary for these values of *St* based on the QLH approximation (Fig. 8).

5.5. Comments on PDF methods

The PDF approach of Zaichik and Alipchenkov (2003) naturally lends itself to the analysis of the net flux at the collision boundary

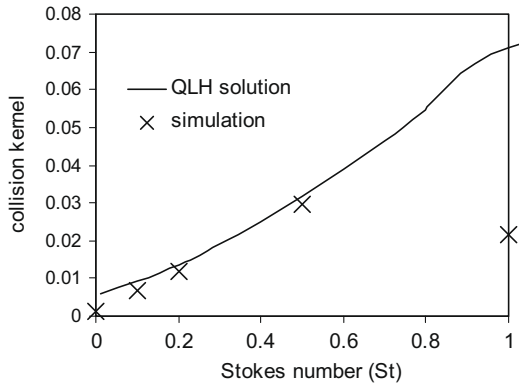

Fig. 23. Comparison between simulation and QLH approximation for the collision kernel.

in terms of a force balance and in particular as the difference between the gradient of the kinetic stresses and the drag force due to the turbulence. This in turn means that the flux is composed of a drift (convective) flux which in this case is proportional to the gradient of the variance of radial velocity fluctuations and a diffusive flux (arising from the drag force due to the turbulence). The probabilistic approach due to Chun et al. (2005) also models the net flux as the sum of a convective flux (Eq. (3)) and a diffusive flux (Eq. (4)). However, the convective flux is explicitly different in form involving the compressibility of the particle velocity field (where the velocity refers to the relative velocity between particle pairs). In the particular case of the random symmetric straining flow we have considered, the particle compressibility for $St \ll 1$ is given by $-2St\dot{\gamma}^2$ and with respect to the principal axes of the flow $\Delta\underline{u} = (\dot{\gamma}x_1(\theta), -\dot{\gamma}x_2(\theta))$ where θ is the orientation of the principal axes to a fixed frame of reference. In the simulation θ and $\dot{\gamma}$ are selected independently at the end of each eddy lifetime, θ from a uniform distribution and $\dot{\gamma}$ from a Gaussian distribution.

$$\underline{v}_d = 2St\langle\dot{\gamma}^3\rangle\langle x_1(\theta), -x_2(\theta)\rangle T_e + O(St^2) \tag{49}$$

where T_e is the eddy lifetime. The first thing to note is that in transforming the components of $\underline{v}_d$ to a fixed frame of reference means that because of the rotation, the first term will vanish independently of whether $\langle\dot{\gamma}^3\rangle = 0$. In our simulations $\langle\dot{\gamma}^3\rangle = 0$. That is $\underline{v}_d = O(St^2)$. Based on the Chun et al. (2005) approach the RDF (for zero absorption at the collision boundary) would go as $r^{-\alpha_{2D}St^2}$ where α_{2D} is a constant. However, our analysis and also that of Zaichik and Alipchenkov (2003) gives r^{-2St} for the RDF from Eq. (40). We strongly suspect that this marked difference in behavior is due to the neglect of a convective term in the closure approximation in Zaichik's kinetic equation and the neglect of contributions from third order moments in the derivation of the drift term given in Chun et al's. (2005), i.e. the derivation is strictly only exact for Gaussian distributions of the random variables involved (see Reeks (2005a) for an improved version of the kinetic equation in inhomogeneous turbulence which involves drift as well as gradient diffusion). This of course will form the subject of further investigation.

6. Conclusions and implications

The random symmetric straining model reproduces the complex behavior of inertial particles interacting with turbulent small scale structures. However, in so doing it is important to recognize that we have ignored the influence of vorticity on the collision rate. A straining flow was chosen to begin with because it is more representative of the flow encountered by particles with $St \sim 1$. Isotropic homogeneous flows ought to contain equal amounts of rotation and straining. Adding a rigid body rotation will compensate for the lack of rotation in a straining flow and can be done for both 2D and 3D with spherical symmetry. The influence of vorticity, how it is correlated with the straining flow will form the basis of a future study. What is important here is that the observed features are consistent with what has been identified in DNS as the mechanisms responsible for the observed dependence of the collision kernel on particle Stokes number (St) peaking with $St \sim 0.5$. One of the two determinant features for the collision kernel is the peaking of concentration near the collision boundary with a maximum around $St \sim 0.25$ corresponding to the value for the critically damped oscillations of individual particles. Note however that for $St \ll 1$ the RDF in this flow field $\sim r^{-\alpha St}$ rather than $r^{-\alpha St^2}$ because of the lack of an equal amount of vorticity along the trajectories of these particles. The second feature causing the particles to agglomerate is the decorrelation of relative velocity between particles or the presence of RUM (Random Uncorrelated Motion) in the flow field which is increasingly important for St larger than a threshold value (Ijzermans et al., submitted for publication) $St \sim 1$ in this work. For sufficiently large Stokes number, velocities between two colliding particles are uncorrelated due to the decorrelation of individual particle velocity from the turbulent flow field corresponding to RUM ~ 1.

By analogy to the deposition in turbulent boundary layer, the increase in collision rate is due to the overshoot of particles which according to free flight theory, are transported by gradient diffusion to within one stop distance of the collision boundary from which point they can coast through their inertia to the collision boundary.

The collision kernel has been compared with the limit for inertialess particles. We obtained a collision kernel much smaller than the prediction of S&T for inertialess particles and $r_c = 0.05$. This is due to the fact that S&T assume a fully mixed condition in the flow domain and here we observed for small particles a significantly lower value for the concentration at the collision boundary than its fully mixed value. Particle transport to the collision boundary is in fact rate-limited by diffusion depending not only upon the turbulent intensity but also upon the choice of the boundary conditions and the turbulent time scale (for most of the cases we considered $\dot{\gamma}T = 1$).

The boundary conditions chosen at the collision boundary were perfectly absorbing which means that particles in this model were removed from the domain after collision in order to reproduce an agglomeration mechanism with 100% efficiency whilst S&T allowed the particles to stay in the domain after collision, i.e. S&T used perfectly reflecting boundary conditions. Fig. 16 clearly showed that considering a perfectly reflecting collision boundary would have enlarged the build-up of the concentration at the collision boundary for intermediate Stokes number and would give the fully mixed condition assumed by S&T for small Stokes number. In contrast, the turbulent time scale was shown to play a significant role for inertial particles, the persistency of the flow reducing the amplitude of the build-up in particle concentration.

The collision kernel calculated from the QLH solution based on a combination of simple gradient diffusion and turbophoresis with the assumption of local homogeneity of the turbulence gives reliable results for $St < 0.5$.

By examining the conservation equations for the momentum at equilibrium we have shown that the build-up of concentration near the collision boundary (as in deposition in a turbulent boundary layer) can be explained at small Stokes numbers in terms of a balance between a convective flux towards the collision boundary due to turbophoresis (proportional to gradient of kinetic stresses (per unit mass)) and turbulent diffusion, For sufficiently large particles, the turbulent diffusion flux becomes negligible and the balance is between the centrifugal drift and the turbophoresis terms.

In the region $r > 0.75$, a sharp rise in the concentration was observed for all Stokes number. This entrance effect observed in sprays is linked to the increasing contribution from the net centrifugal force which compensates for the reduction in the diffusive term $\langle \rho u_r \rangle$. The positive sign of $\langle \rho u_r \rangle$ for a positive gradient of concentration suggests a negative diffusion coefficient, such features having been observed in analytic solutions of particle dispersion in simple straining flows (Reeks, 2005b).

The form of the velocity distribution calculated at the collision boundary which is clearly not half Gaussian as often assumed in PDF approach can be directly used to obtain the explicit solution of the PDF equation given by Eq. (1).

The results presented in this work are strictly appropriate for the concentration scaling on $r_c/R \ll 1$ (i.e. the concentration is influenced only by the flow close to the collision boundary) In fact for small Stokes numbers, the concentration profile near the collision boundary only depends on the ratio r_c/R independent of R as suggested by Fig. 15. However, for sufficiently large St it is influenced by the whole straining region from r_c to R. In order to compare the results to DNS results in the literature the symmetric straining flow field should be therefore extended from 2-dimensions to 3. We also need to simulate the entire structure function $\langle \Delta u^2(r) \rangle$ and at the same time satisfy continuity of flow for each realization of the flow (to avoid spurious drift) These are problems common to simulating deposition in turbulent boundary layers other than by DNS. We should finally note that the simulation is for particles of the same size. Simulations for the collision of different size particles should take account of the motion of their centre of mass (see Chun et al., 2005).

References

Bec, J., 2005. Multifractal concentrations of inertial particles in smooth random flows. J. Fluid Mech. 528, 255–277.

Brunk, K.B., Koch, D.L., Lion, L.W., 1998. Turbulent coagulation of colloidal particles. J. Fluid Mech. 364, 81–113.

Chun, J., Koch, D.L., Rani, S., Ahluwalia, S., Collins, L.R., 2005. Clustering of aerosol particles in isotropic turbulence. J. Fluid Mech. 536, 219–251.

Crowe, C.T., Chung, J.N., Troutt, T.R., 1993. Particle dispersion by organized turbulent structures. In: Roco, M.C. (Ed.), Particulate Two-Phase Flow, Butterworth-Heinemann, Stoneham, MA.

Falkovich, G., Fouxon, A., Stepanov, M.G., 2002. Acceleration of rain initiation by cloud turbulence. Nature 419, 151–154.

Fevrier, P., Simonin, O., Squires, K.D., 2005. Partitioning of particle velocities in gas–solid turbulent flows into a continuous field and a spatially uncorrelated random distribution: theoretical formalism and numerical study. J. Fluid Mech. 533, 1–46.

Fung, J.C.H., 1993. Gravitational settling of particles and bubbles in homogeneous turbulence. J. Geophys. Resour. 98, 287–297.

Güntay, S., Suckow, D., 2004. ARTIST: introduction and first results. Nucl. Eng. Des. 1, 109–120.

Ijzermans, H.A.R., Reeks, M.W., Meneguz, E., submitted for publication. Segregation and dispersion of inertial particles in simple random flows. J. Fluid Mech.

Liu, B.Y., Ilori, T.A., 1974. Aerosol deposition in turbulent pipe flow. Environ. Sci. Tech. 8, 351–356.

Maxey, M.R., 1987. The gravitational settling of aerosol particles in homogeneous turbulence and random flow fields. J. Fluid Mech. 174, 441–465.

Pinsky, M., Khain, A.P., 2000. Stochastic effects of cloud droplet hydrodynamic interaction in a turbulent flow. J. Atmos. Res. 53, 131–169.

Pope, S.B., 2000. Turbulent Flows. Cambridge University Press, Cambridge, UK.

Reade, W.C., Collins, L.R., 2000. A numerical study of the particle size distribution of an aerosol undergoing turbulent coagulation. J. Fluid Mech. 415, 45–64.

Reeks, M.W., 2005a. On model equations for particle dispersion in inhomogeneous turbulence. Int. J. Multiphase Flow 31, 93–114.

Reeks, M.W., 2005b. On probability density function equations for particle dispersion in inhomogeneous turbulence. J. Fluid Mech. 522, 263–302.

Reeks, M.W., Simonin, O., 2006. Multiphase flow handbook. In: Crowe, C.T. (Ed.), PDF Models. CRC Press, Berlin.

Saffman, P.G., Turner, J.S., 1956. On the collision of drops in turbulent clouds. J. Fluid Mech. 1, 16–30.

Shaw, R.A., Reade, W.C., Collins, L.R., 1998. Preferential concentration of cloud droplets by turbulence: effects on the early evolution of cumulus cloud droplet spectra. J. Atmos. Sci. 55, 1965–1976.

Simonin, O., 1996. Combustion and Turbulence in Two-Phase Flows, von Karman Institute for Fluid Dynamics. Lecture Series 1996-02.

Squires, K.D., Eaton, J.K., 1991. Preferential concentration of particles by turbulence. Phys. Fluids A3, 1169–1178.

Sundaram, S., Collins, L.R., 1997. Collision statistics in an isotropic particle-laden turbulent suspension. Part 1. Direct numerical simulations. J. Fluid Mech. 335, 75–109.

Vaillancourt, P.A., Yau, M.K., 2000. Review of particle–turbulence interactions and consequences for cloud physics. Bull. Am. Meterol. Soc. 81, 285–298.

Wang, L.P., Wexler, A.S., Zhou, Y., 1998a. On the collision rate of small particles in isotropic turbulence. I. Zero-inertia case. Phys. Fluids 10, 266–276.

Wang, L., Wexler, A.S., Zhou, Y., 1998b. On the collision rate of small particles in isotropic turbulence. II. Finite inertia case. Phys. Fluids 10, 1206–1216.

Wang, L.P., Ayala, O., 2005. Theoretical formulation of collision rate of cloud droplets in turbulent atmosphere. J. Atmos. Sci. 62, 2433–2450.

Wang, L.P., Maxey, M.R., 1993. Settling velocity and concentration distribution of heavy particles in homogeneous isotropic turbulence. J. Fluid Mech. 256, 27–68.

Wilkinson, M., Mehlig, B., Bezuglyy, V., 2006. Caustic activation of rain showers. Phys. Rev. Lett. 97, 048501.

Young, J.B., Leeming, A., 1997. Theory of particle deposition in turbulent pipe flow. J. Fluid Mech. 340, 129–159.

Zaichik, L.I., Alipchenkov, V.M., 2003. Pair dispersion and preferential concentration of particles in isotropic turbulence. Phys. Fluids 15, 1776–1787.

Zaichik, L.I., Alipchenkov, V.M., 2005. Statistical models for predicting particle dispersion and preferential concentration in turbulent flows. Int. J. Heat Fluid Flow 26, 416–430.

Zaichik, L.I., Alipchenkov, V.M., 2006. Modelling turbulent collision rates of inertial particles. Int. J. Heat Fluid Flow 27, 937–944.

Zaichik, L.I., Simonin, O., 2006. Collision rates of bidisperse inertial particles in isotropic turbulence. Phys. Fluids 18, 035110.